ELSEVIER

Contents lists available at ScienceDirect

International Journal of Mechanical Sciences

journal homepage: www.elsevier.com/locate/ijmecsci





A fully discrete element approach for modeling vacuum packed particle dampers

Pawel Chodkiewicz ap, Robert Zalewski p, Jakub Lengiewicz b, **

- ^a Warsaw University of Technology, Narbutta 84, Warsaw, 02-524, Poland
- b Institute of Fundamental Technological Research, Polish Academy of Sciences, Pawinskiego 5B, Warsaw, 02-106, Poland

ARTICLE INFO

Keywords: Discrete element method Simulations Granular damper VPP Vacuum-packed particles YADE DEM

ABSTRACT

In this work, we investigate Vacuum-Packed Particle (VPP) dampers — granular-core dampers offering tunable damping performance under varying vacuum levels. A comprehensive computational model of the entire VPP damper system is developed using the Discrete Element Method (DEM). A novel discrete-element model of the flexible foil, responsible for consistently transmitting the external pressure resulting from vacuum application, is introduced and implemented by extending the open-source Yade DEM framework. A prototype VPP damper is also designed and experimentally tested, enabling both model calibration and validation of the simulation results. The calibrated DEM model is subsequently employed in a parametric study to assess the influence of material, geometrical, and process parameters on damper performance. All code, along with the associated experimental and simulation datasets, is made available in an open-access repository.

1. Introduction

In recent decades, growing awareness of environmental issues and the urgent need to comply with evolving ecological standards have fueled the pursuit of more sustainable solutions across various industrial sectors. Researchers and engineers are increasingly seeking innovations that integrate eco-friendly "smart" materials capable of adapting their properties in response to changing conditions. Such efforts aim to reduce harmful emissions, promote recycling processes, and ultimately revolutionize engineering practices for a greener and more efficient future [1,2].

Within this broad class of adaptive and eco-conscious technologies, particulate or granulate materials have garnered significant interest. Granular media can exhibit remarkable behaviors [3–7] such as jamming transitions, enhanced energy dissipation [8], and tunable mechanical properties. These characteristics enable their use in a wide range of applications, including blast-mitigation seats in military vehicles [9], medical devices for endoscopic support [10,11], haptic rehabilitation tools [12], adaptive sound-absorbing systems [13], reconfigurable crash energy absorbers [14,15], and flexible grippers in soft robotics [16–18]. Moreover, the potential to incorporate recycled or natural fillers into granular cores places these materials squarely within the sustainable product life cycle.

This study focuses specifically on Vacuum-Packed Particle (VPP) dampers [19,20] — granular-material-based systems of tunable mechanical damping properties. By leveraging the jamming effect under

vacuum, these dampers can transition between quasi-fluid and viscoplastic states, providing a controllable means of vibration damping and impact energy absorption. Moreover, VPP dampers have a relatively simple structure and can be filled with a wide array of granulate media, including those derived from recycled or naturally sourced materials [21]. For certain applications, such versatility can make VPP dampers a promising alternative to traditional magnetorheological (MR) or electrorheological (ER) damper devices in applications where simplicity, cost-effectiveness, and environmental compatibility are critical [22,23], while rapid transient responses are not that crucial.

Characterizing and optimizing granular systems demand advanced mathematical, numerical, and experimental methods. Granular media are inherently complex due to their sensitivity to factors such as humidity, temperature, strain rate, and the interplay of various physical fields. While commercial simulation packages (e.g., LS-Dyna [24] or SolidWorks [25]) offer robust tools for macroscopic materials, they are typically less adept at capturing the intricate particle-scale interactions central to granular mechanics. Engineers require specialized methods to accurately capture phenomena such as friction, inter-particle contact forces, and jamming transitions. Thus, precise calibration against experimental data and specialized modeling tools are often indispensable when developing novel devices based on granular media.

The Discrete Element Method (DEM) [26,27] stands out as a particularly suitable modeling framework for studying particulate systems, given its ability to treat each particle as a separate entity. Alternative

E-mail address: jleng@ippt.pan.pl (J. Lengiewicz).

^{*} Corresponding author.

particle-continuum approaches such as the Material Point Method (MPM) [28] or the Particle Finite Element Method (PFEM) [29] could in principle also be used to model VPP dampers. However, these methods require background grids or frequent remeshing and would need to be coupled with DEM for the granular core, making their application less straightforward in this context. DEM has been successfully employed in diverse applications: simulating filtration processes with dry and wet approaches [30,31], analyzing fluid flow in pre-cracked rock specimens under high pressure [32], and modeling electrical conduction in partially sintered porous materials [33]. It has also proven effective in investigating the damping performance of layered beams with a granular core [34], developing distributed modular robotic systems with reconfigurable mechanical properties [35-37], and analyzing extreme loading scenarios in materials such as concrete [38]. Furthermore, DEM-based studies have been conducted to evaluate the micro-macro behavior of geomaterials under traffic, wave, and earthquake loads [39-41].

In our work, we consider VPP damper systems, which rely on interaction between the discrete phase (granulate) and the continuous phase (foil envelope). For studying such more complex scenarios, usually specialized coupling libraries, such as preCICE [42], are utilized to combine dedicated simulation environments for each of the involved phases, see, e.g., fluid-particle-structure interactions [43,44], or comprehensive commercial libraries such as FLAC3D in which DEM-FEM coupling can be applied to model flexible membranes [45], including FEM shell elements . In the present work, instead, we model the entire foil-granulate system within a single open-source DEM simulation environment. In particular, we develop an extended DEM model that discretizes the elastic foil within the DEM framework, and allows to model its response to mechanical loads and surface pressure loads. We note that similar DEM-based strategies for representing flexible membranes or confining boundaries have been extensively applied in geomechanics, particularly in DEM simulations of triaxial tests [46-51]. Our approach differs in that it introduces a lightweight squarebased arrangement of foil particles with regular vacancies, designed to provide robust predictions at a reduced computational cost, and tailored to the cyclic loading conditions of VPP dampers. This approach follows our earlier first attempts [52], and provides a robust alternative that demonstrated very good predictive capabilities. We implement the proposed novel DEM-based approach in the open-source Yade DEM framework [53,54].

The present work focuses on both the experimental and numerical investigation of VPP dampers under a variety of operating conditions. The new DEM tool is used to fit experimental data and to examine how various design parameters – such as particle stiffness, frictional properties, and vacuum level – affect the overall damping characteristics of VPP systems. As such, our new modeling approach complements prior analytical and semi-empirical studies that employed constitutive equations calibrated with experimental data and advanced algorithmic methods [20,22,23,55,56].

The remainder of this paper is organized as follows. Section 2 details the experimental setup and procedures used to characterize the mechanical response of the VPP dampers. Section 3 introduces the DEM-based numerical model, describing the contact laws, boundary conditions, and calibration strategies. Section 4 presents a comparative analysis of the experimental and numerical results, examines the effectiveness of the proposed modeling approach, and provides a parametric study of various VPP damper settings. Finally, Section 5 concludes the paper with a summary of the main insights and potential future directions.

2. VPP damper experiment

A VPP damper, in its simplest form without any internal spring, consists of a flexible foil shell and loose particles sealed under reduced air pressure. The foil, which is an airtight and durable polymer film, is

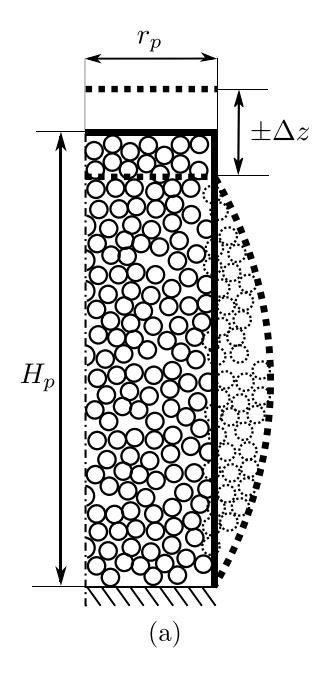
typically shaped into a cylindrical envelope and filled with a granular medium, see Fig. 1. In this study, polymer spherical granules are used for that purpose, although virtually any particle type or shape can be employed [21]. Once the granulate is in place, the air inside the envelope is partially evacuated to create a pressure difference. This reduction in internal pressure causes the particles to compact and lock together through frictional and interlocking forces, effectively transitioning the material from a fluid-like state to a quasi-solid or rigid state. Consequently, the damper exhibits enhanced stiffness and damping characteristics under vacuum, as the granules are no longer free to move independently when subjected to external mechanical loading. Furthermore, the level of underpressure can be controlled, allowing to modulate the energy dissipation performance under oscillatory motion.

In the experiment, we use a VPP damper with a height of $H_{\rm p}=100~{\rm mm}$ and a radius of $r_{\rm p}=25.5~{\rm mm}$, and the foil thickness of $t_{\rm f}=0.15~{\rm mm}$. The geometry of the setup is presented in Fig. 1 and the list of calibrated parameters is provided in Table 1. The experimental procedure consists of the following steps:

- 1. **Filling the envelope:** The foil envelope is filled with spherical granules.
- Compression and re-filling: The granulate is iteratively compressed and re-filled to achieve a higher packing density. (The volume ratio was measured *a posteriori*, after the experiment concluded.)
- Sealing the sample: The sample is capped and sealed at both ends, with the upper cap integrated into a compressor that controls the underpressure level within the sample.
- Mounting in the Testing Machine: The sample is placed in the grips of the SHIMADZU EZ-LX testing machine equipped with a 5000 kN force load cell.
- 5. **Pressure Stabilization:** The underpressure is set to one of four distinct values, Δp , of 0.02 MPa, 0.04 MPa, 0.06 MPa, and 0.08 MPa, corresponding to 20%, 40%, 60%, and 80% of atmospheric pressure, respectively.
- 6. **Cyclic Loading:** Under a constant quasi-static strain rate and a triangular excitation protocol, the sample is subjected to cyclic compression and tension over a displacement amplitude of $\Delta z = 10$ mm. Throughout this process, the underpressure level is maintained, and time, yaw displacement, and force data are recorded throughout the cycles. (The initial force is calibrated to 0 N.)

The experiments presented in this work were conducted within an underpressure range of 0.02–0.08 MPa, with the aim of positioning VPP structures as alternatives to semi-active vibration damping devices. The lower limit of 0.02 MPa is based on our previous empirical experience, from which a fully developed jamming mechanism can be assumed; this is further supported by recent observations [20]. The theoretical upper limit corresponds to a technical vacuum of approximately 0.1 MPa. In practice, however, the attainable limit is constrained by the capacity of commercially available vacuum pumps – which influences both the maximum achievable vacuum level and the response time – as well as by the difficulty of maintaining airtightness in VPP damper chambers at near-vacuum conditions.

The results of the experiment are shown in Fig. 2. We can observe a significant effect of the underpressure level on energy dissipation, with higher underpressure yielding larger hysteresis loops. This effect allows for tuning of the system: by adjusting the partial vacuum within the device, one can control its overall mechanical properties. Another observation is that, after the short initial phase, the process stabilizes, and the system maintains consistent energy dissipation characteristics over subsequent cycles. These observations confirm the robustness of VPP dampers, and underscore its potential for applications requiring adaptable damping characteristics.



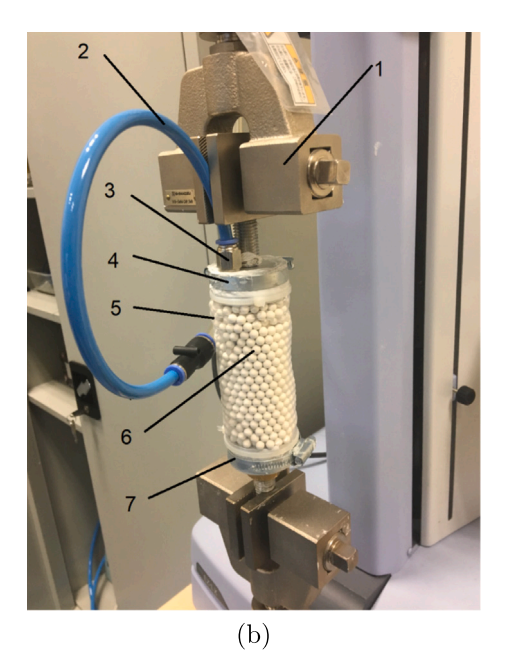


Fig. 1. VPP sample testing stand. (a) schematics of the VPP damper with the dashed line indicating the compressed geometry, (b) the VPP damper fixed in the strength testing machine (1–grips of the testing machine; 2–tube connecting the specimen to the vacuum pump; 3–valve; 4–upper rigid cap of the specimen; 5–flexible membrane; 6–spherical granules; 7–lower cap of the specimen).

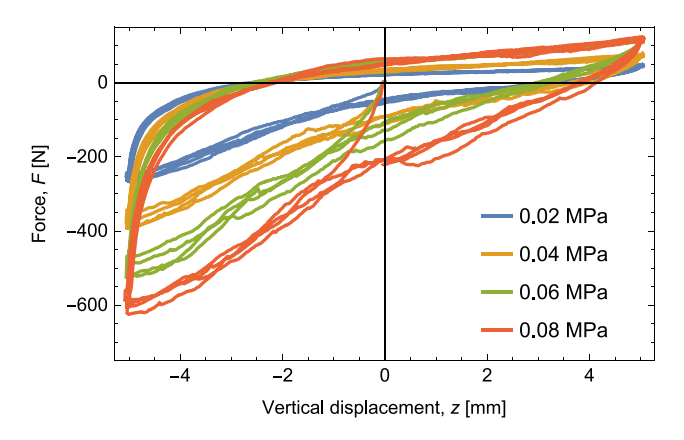


Fig. 2. Experimental results for four different underpressure levels Δp , which represents the pressure difference between the atmospheric pressure and the pressure inside the damper. The hysteresis loops for the first four cycles are shown for each case.

3. DEM modeling

In the presented approach, the mechanical response of the VPP damper system is modeled using an explicit Discrete Element Method (DEM) framework implemented in Yade [53,54,57]. This section briefly summarizes the essential DEM operations, see Section 3.1, and then describes our novel approach to representing the flexible foil as a two-dimensional network of spherical particles, see Sections 3.2 and 3.3. All code, together with the experimental and simulation datasets, is made available in open-access repositories [58,59].

3.1. DEM simulation framework

In our DEM model of VPP damper, we distinguish tree types of entities: the particles of granulate, the particles used to discretize foil, and the rigid planes/segments to model the upper and lower capping of the VPP sample. All contact interactions are implemented within the classical Cundall–Strack linear spring–dashpot model [60], see

also [57] For the interactions between the granulate particles we use the Coulomb friction law (i.e., linear springs in the normal and tangential directions with sliding governed by the Coulomb criterion). The interaction between the particles of foil are of adhesive type, allowing for modeling permanent bonds that represent the elastic response of foil (see also Sections 3.2 and 4); the maximum bond strength was set sufficiently high that no bond breakage occurs under the studied loading conditions, so the foil network remains continuous. The third type of interaction is between the granulate and the walls (i.e., the foil and the upper/lower capping). In real system, these interactions involve friction, however, in the current DEM model, we decided to model the granulate-foil interaction as frictionless. This means that in the Cundall-Strack law the tangential stiffness and friction coefficient were set to zero for grain-foil contacts. The reason for that is that, in our approach, the originally smooth foil is discretized as a "rough" layer of DEM particles, therefore, there exist a dilatant interlocking between the granulate and foil particles. This granulate-foil interlocking provokes the friction-like resistance in sliding, even when no granulate-foil friction is present.

After the VPP damper DEM geometry is established, the multi-step DEM analysis is performed. In the analysis, at a given time step, the following sequence of actions is performed:

- Collision detection: Identify when two particles come into potential contact based on their positions and radii.
- 2. **Interaction initialization and property assignment:** Create the interaction and determine its properties, such as stiffness. This is done either through precomputed values or derived from the physical properties of the interacting particles.
- Interaction physics: For interactions already established in previous time steps, perform the following computations:
 - (a) Strain evaluation: Calculate the deformation of the interaction based on relative particle displacement.
 - (b) Force computation: Determine forces as functions of the calculated strains and external loadings, using materialspecific constitutive models. The particular example of external loading due to the pressure difference is presented in Section 3.3.

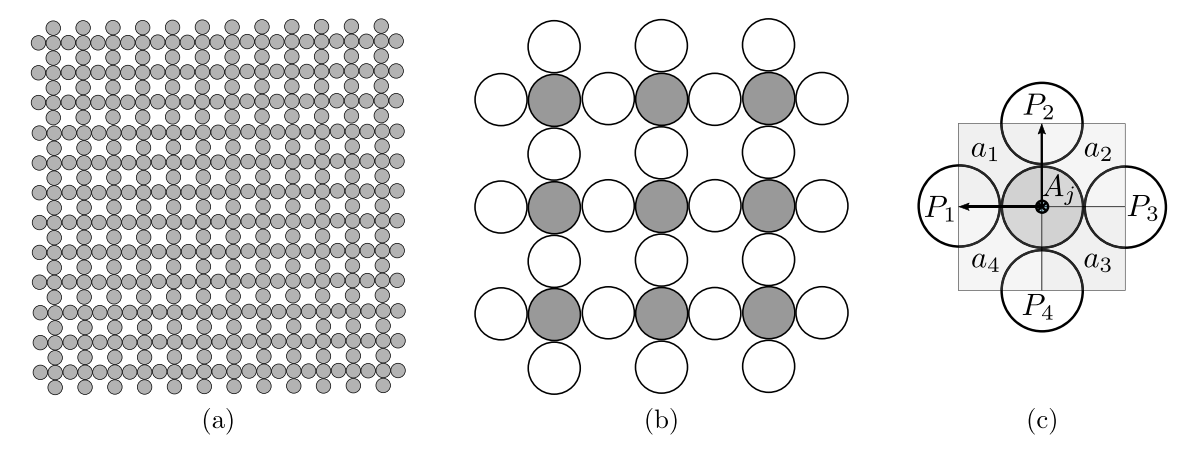


Fig. 3. Schematic of the arrangement of particles in the membrane (a). In the zoom-in (b), the particles used to apply pressure difference are marked in gray color. In (c), the elementary cell j is shown, with the notation used for calculating the surface area vector \mathbf{A}_j .

4. Force application: Apply the computed forces to the particles involved in the interaction to update their motion and positions. Increment the time, apply the Dirichlet boundary conditions, and proceed to the Step 1.

This sequence is repeated until the simulated process finishes, e.g., a desired number of loading cycles is performed.

Remark. We acknowledge that in DEM, large overlaps may occur under very high confinement. In our case, however, the loading conditions reproduced the experimental setups and produced global deformations well below 10%. At such strain levels, the particle overlaps inherent to the Cundall–Strack linear contact model remained small relative to particle size. In addition, the deformable foil wrapper redistributed local stresses and prevented abnormal buildup of contact forces, while the perforation size of the foil was chosen to be much smaller than the grain diameter, so that no particle could pass through. Consistent with these considerations, during all simulations we did not observe any particle escape or signs of instability.

3.2. DEM modeling of flexible foil: elastic model

We model the flexible foil membrane as a two-dimensional network of interconnected spherical particles. There are countless possibilities in which circular particles can be arranged in two-dimensional space [61–63], with square- and hexagonal packings being the most popular choices. When making that choice in our particular case, we were aiming to achieve a lightweight DEM representation of foil that will assure robust and accurate predictions at a minimum additional computational burden. This led us to the square-based arrangement of foil particles that contains regular vacancies, see Fig. 3a. Although the presence of vacancies in the square-based network may create an increased tendency to lock granulate particles (which is partially mitigated by setting frictionless foil-granulate interaction), it provides several modeling advantages as described below.

This special particle arrangement serves for several purposes. Firstly, the choice of the square packing is less dense as compared to the hexagonal packing, which is additionally optimized by removing selected 25% of particles, allowing for a significant reduction in computation time. Secondly, the removal of some particles provides more flexibility to the foil membrane, which is now more capable to adapt effectively to the shape of the granules within the sample, which allows to optimally transmit forces associated with the pressure difference. Lastly, the remaining network of particles that form the foil is able to accurately represent the elastic properties of foil and to transmit and re-distribute forces associated with the cyclic loading of VPP damper.

The orthogonal orientation of the particle network in the cylindrical VPP envelope is chosen such that the main symmetry axis coincides with the longitudinal and circumferential directions of the cylinder, see also Fig. 4. These are the two main directions that transmit the tensile forces in the discretized foil. In order to create the relationship between the elastic modulus of real (continuous) foil, E_v , and the elastic modulus of its simplified discretized model, $E_{\rm s}$, we need to consider two effects. The first effect is related to the fact that there are vacancies in the discretized model, and only every second column/row can transmit the forces. This makes it necessary to effectively increase the elastic modulus of the discretized model by the factor of 2 with respect to the continuum counterpart. The second effect is related to difference between the thickness of the real foil, $t_{\rm f}$, and the apparent thickness of the discretized model which is the diameter of the foil particle, $2 \cdot r_s$. The elastic modulus must be accordingly scaled to account for that. The final formula for the corrected elastic modulus reads

$$E_{\rm s} = 2 \cdot E_{\rm y} \cdot \frac{t_{\rm f}}{2 \cdot r_{\rm c}}.\tag{1}$$

3.3. DEM modeling of flexible foil: vacuum pressure

As explained in Section 2, the operation of Vacuum Packed Particle dampers is controlled by the level of vacuum inside the envelope. This results in external pressure that is transmitted to the granulate through the foil envelope. In the DEM simulation, this external loading can be applied as forces acting at foil particles in the direction perpendicular to the current surface of the membrane.

In the case of foil discretization proposed in this work, the forces originating in pressure difference are only applied to the foil particles that are at the intersection of perpendicular chains forming the network, see gray particles in Fig. 3b. This choice is motivated by the fact that, for the particles at the intersection, it is straightforward to determine the tributary area vector that is necessary to produce the force vector. The remaining foil particles (white in Fig. 3b) only experience the pressure-difference force indirectly through their adhesive connections to the loaded particles. Even though this heuristic is only an approximation, it proved to be sufficient to capture the pressure dependence of VPP damper responses, as shown later in this work.

For the proposed regular geometry, the tributary surface area vector \mathbf{A}_j of the foil particle \mathbf{S}_j is the sum of respective contributions from four neighboring segments:

$$A_j = \sum_{i=1}^4 a_i,$$
 $a_i = (P_i - S_j) \times (P_{1+(i\%4)} - S_j)$ (2)

where S_j is the position of the central (gray) particle, % is the modulo operation, and P_i is the position of the *i*th neighboring particle, see

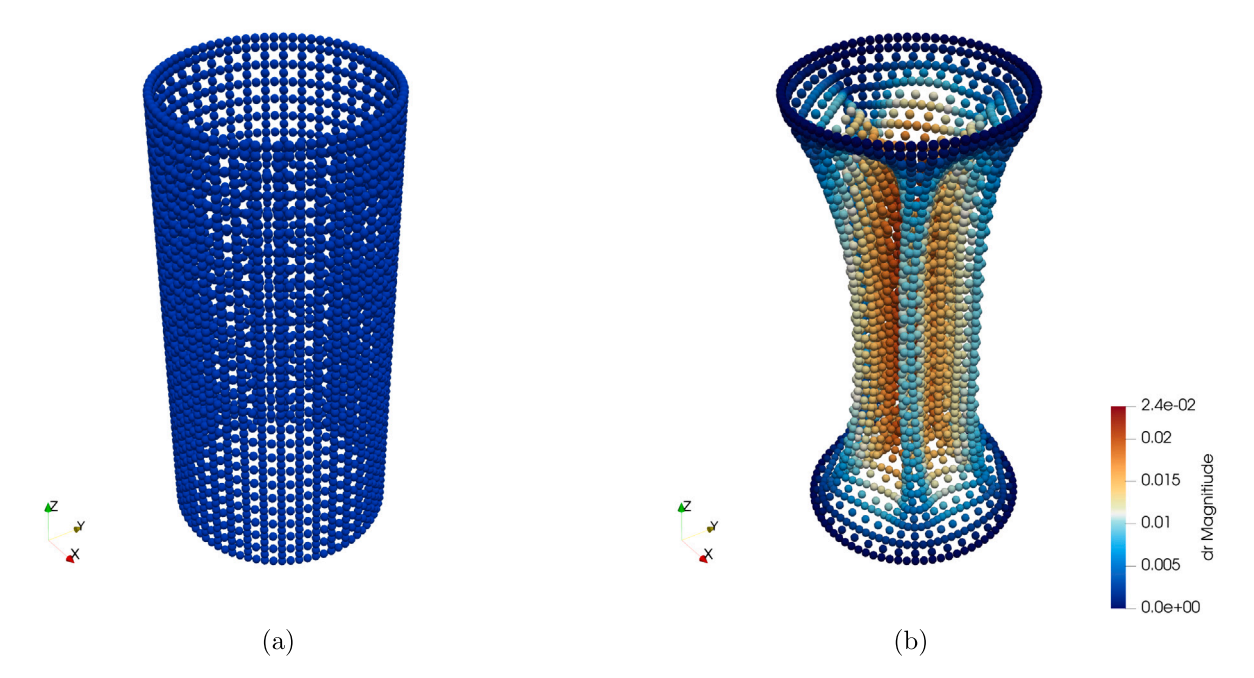


Fig. 4. Simulation of an empty foil envelope subjected to an underpressure corresponding to the 10% reduction with respect to the atmospheric pressure ($\Delta p = 0.01$ MPa). (a) Initial configuration. (b) Loaded configuration. The colors represent the magnitude of radial component of the displacement (i.e., the change of distance from the central axis).

Fig. 3c. A_j is pointing outwards to the membrane surface, and depends on the current position of the contributing particles. For such a defined tributary area vector, the force applied on a foil particle S_j is equal to

$$F_{j} = -\Delta p \mathbf{A}_{j},\tag{3}$$

where Δp is the pressure difference (positive for the underpressure).

4. Model calibration, performance and parametric study

This section provides an empirical demonstration of the fitting and predictive capabilities of the proposed DEM model. In Section 4.1, we outline the steps to set up the Yade DEM simulation to represent the experimental setup. Section 4.2 details the calibration of the DEM model parameters using experimental data. Finally, Section 4.3 validates the predictive performance of the calibrated model, and examines the influence of material, design, and process parameters on VPP damper performance.

4.1. DEM analysis for VPP damper

In the DEM analysis, we aim to accurately simulate the laboratory tests of the VPP damper described in Section 2. We begin with setting up the foil membrane by arranging the particles to form the cylindrical shape, as illustrated in Fig. 4, following the arrangement topology discussed in Section 3.2. The number of particles in the circumferential direction is adjusted such that the radius of the DEM model is as close as possible to the real radius, $r_{\rm p}$, used in the experiment. The upper and lower layers of the foil are fixed, which allows us to control their positions during the simulation.

Having the membrane geometry ready, we perform a sanity check of the proposed novel mechanism of applying pressure difference (see also Section 3.3 for the details of DEM formulation). In this simple qualitative test, we used an empty foil envelope and applied various levels of pressure or underpressure. The test confirmed the expected behavior of the model. For instance, the result for a moderate level of underpressure is presented in Fig. 4(b), showing a squeezed deformation pattern with

several visible buckling folds, which also involves the self-contact of the foil folds.

In the next step, the empty membrane is filled with the granulate by letting the granules naturally fall under the gravity forces. To ensure complete filling of the sample to a desired packing ratio of 54%, the necessary amount of granulate is created and directed into the membrane through a special temporary "funnel" structure that is constructed with triangular rigid facets. During the filling process, the friction between the granulates is reduced to zero to facilitate their free movement, and consequently allowing for a non-obstructed filling of the entire foil structure. As the last step, a rigid capping is moved downwards until a designed damper's height, $H_{\rm p}$, to additionally enforce the granulates' rearrangement. The state after this process is visualized in Fig. 5a.

The main loading cycles in the simulation are carried out by applying a sawtooth-shaped vertical displacement with an amplitude of $\Delta z =$ 10 mm to the upper wall and the top ring of foil particles (see two peak configurations in Fig. 5(b-c)). This represents the experimental setup in which the foil is attached to the moving top cap and the granulate interacts with the cap via the unilateral contact. The loading velocity is set to $v_{\rm z}=33.3\times 10^{-5}\,{\rm m/s}$ (see also the parametric study in Section 4.3 and Fig. 12). The vertical reaction forces are captured individually at the upper wall and at the fixed top foil ring, which allows their individual contributions to be observed; see also Fig. 7. The forces are sampled 500 times per cycle (i.e., every 0.12 s) by averaging over the interval 2×10^{-4} s, where $t_c = 2\Delta z/v_z \approx 60$ s is the duration of a single loading cycle, while the time increment in the DEM analysis is set to approximately 2×10^{-6} s. The time increment was determined using the PWaveTimeStep() function available in the YADE framework, which computes a numerically stable increment based on the P-wave velocity, itself dependent on particle stiffness (Young's modulus), density, and diameter. Although different particle types were present in the system, the foil particles governed the critical timestep; since their properties remained constant, the same increment was used in all cases analyzed.

4.2. Calibration of the parameters of VPP damper model

The DEM model of the VPP damper includes several material and geometrical parameters, accompanied by the respective process parameters, as summarized in Table 1. Most of these parameters were

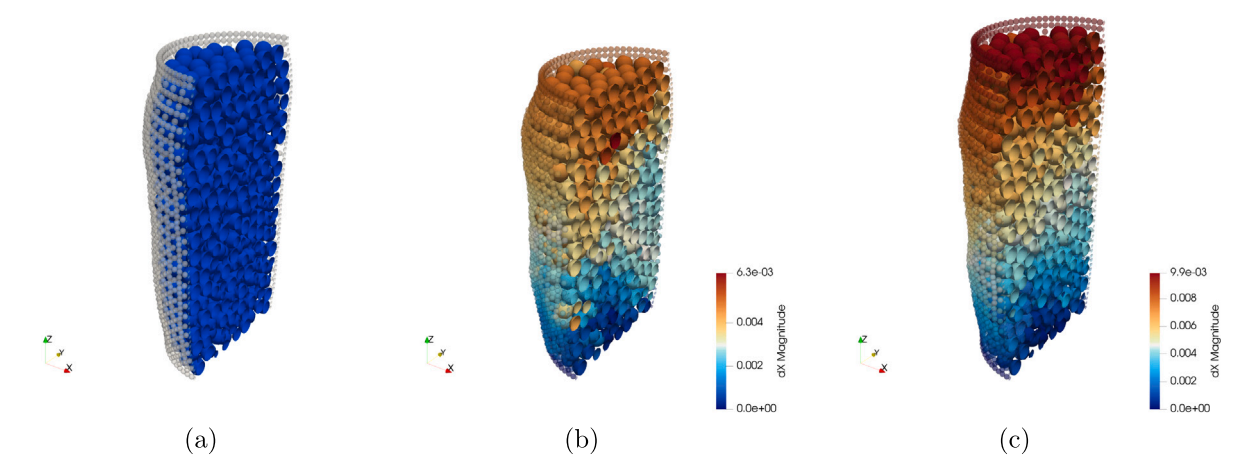


Fig. 5. Three stages of the simulation. (a) The filled sample, after allowing the granulate to fall freely under gravity and then compressing them by the upper wall. (b) The configuration compressed from (a) by 5 mm. Colors represent the displacement magnitude, $\|x_b - x_a\|$, between the configurations (b) and (a). (c) The configuration unloaded from (b) by 10 mm. Colors represent the displacement magnitude, $\|x_c - x_b\|$, between the configurations (c) and (b).

Table 1Calibrated parameters of the VPP damper.

| Parameter | Symbol | Value | Unit |
|---|------------------|------------------------|-------------------|
| Granulate: particle radius | $r_{ m k}$ | 2.965×10^{-3} | m |
| Granulate: particle density | $ ho_{ m k}$ | 2689.639 | kg/m ³ |
| Granulate: particle Young modulus | $E_{ m k}$ | 2300 | MPa |
| Granulate: particle friction coefficient | $\mu_{ m k}$ | 0.6 | - |
| Granulate: volume ratio of grains | | 54% | - |
| Membrane: foil thickness | t_{f} | 0.15×10^{-3} | m |
| Membrane: particle radius | $r_{ m f}$ | $r_{\rm k}/3$ | m |
| Membrane: material density | $ ho_{ m f}$ | 151.77 | kg/m ³ |
| Membrane: particle Young modulus (Eq. (1)) | E_{s} | 18.545 | MPa |
| Membrane: real foil Young modulus | $E_{ m f}$ | 122.18 | MPa |
| Membrane: friction coefficient of particles | $\mu_{ m f}$ | 0 | - |
| Process: amplitude of excitation | Δz | 10.0×10^{-3} | m |
| Process: loading velocity | $v_{\rm z}$ | 33.3×10^{-5} | m/s |

obtained through direct measurements. Regarding the granulate, the granulate radius $r_{\rm k}$ and density $\rho_{\rm k}$ represent average values calculated from measurements performed on a sample of 100 particles. The Young modulus of the granulate was taken from the manufacturer's specification. This approach is justified because, as demonstrated by the parametric study presented in Fig. 11, the response of the VPP damper remains insensitive to variations in the Young modulus across a wide range of values.

The foil parameters, such as thickness and density, were determined through direct measurements. The Young modulus of the foil was obtained via an auxiliary dedicated physical experiment in which a rectangular foil membrane was subjected to a uniaxial tensile test. The experimentally determined elastic modulus, E_y , was then transformed via Eq. (1) to the corrected elastic modulus, E_s , of foil particles. The DEM parameters of foil were validated by carrying out a simple DEM simulation, see Fig. 6(a), which indicated a very good agreement between the experimental data and the model predictions, as shown in Fig. 6(b).

The above-mentioned procedure allowed the determination of all model parameters except for the friction coefficient between granulate particles, μ_k . The friction coefficient, when obtained from direct experimental measurement, was at the level of 0.2, which could not provide a sufficiently precise fit between the VPP damper experiment and the DEM simulation. One of the reasons for that could be geometrical inhomogeneities of the particles' surface, leading to a more pronounced frictional response under the multi-axial load conditions. The problem of fitting the friction coefficient for particle damping systems has also been observed by other researchers [8]. To alleviate that problem, we calibrated the friction coefficient by fitting the results of the DEM

simulation (outlined in Section 4.1) to the experimental data shown in Fig. 2. Calibration was conducted only for the single underpressure level of $\Delta p=0.06$ MPa, employing a grid search for friction coefficient values $\mu_{\rm k}$ ranging from 0 to 1 (the parametric study for various friction coefficients, which served for the grid search, is shown in Fig. 10). As a result, $\mu_{\rm k}=0.6$ has been identified as the best fit.

The calibration results for $\Delta p=0.06$ MPa are presented in Fig. 7, along with a detailed breakdown for the individual reaction force contributions from foil and granulate. For the foil contribution, we recorded the total z-component of the reaction force at the top ring, which represents the vertical pulling force (positive) exerted by the rest of the foil. For the grain contribution, we recorded the compressive reaction force (negative) at the upper wall, reflecting its direct contact interactions with the grains. Such decomposition, obtainable only through the DEM simulation, offers deeper insights into the respective roles of these two main components of the VPP damper. The comparison demonstrates very good qualitative and quantitative agreement between simulation and experimental results. Slight discrepancies, observed at the onset of compression phase, may stem from operational limitations of the vacuum pump, which struggled to keep pace with the decreasing sample's volume.

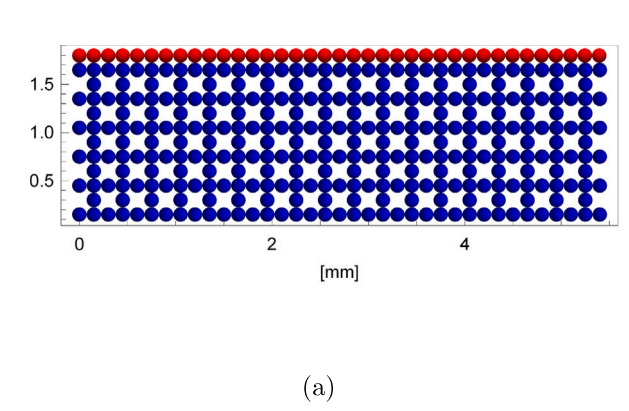
Remark. The initial loading phase starting from the nominal zero position (see Fig. 2, where the lines originate from the coordinate system origin) was intentionally omitted in the calibration and subsequent analysis in order to exclude seating effects and initial prestress. The presented curves therefore reflect the stabilized hysteresis behavior, typically observed from the 2nd–3rd cycle onward.

To assess the generalization capability of the fitted model, Fig. 8 illustrates how it reproduces experimental hysteresis loops for vacuum pressure levels not included in the calibration dataset. The model shows very good predictive performance overall, with a slight deviation observed for the lowest vacuum pressure case, $\Delta p = 0.02$ MPa.

To complement this qualitative comparison and generalization study, we also provide a compact quantitative evaluation of the agreement between experimental measurements and DEM simulations. Specifically, we introduce two metrics: the energy dissipation per cycle, W, and the effective loading stiffness, k. Both are computed from the force–displacement dataset, (z_i, F_i) , representing the damper's response over one loading cycle. The energy dissipation per cycle is defined as:

$$W = \frac{1}{2} \sum_{i=1}^{n} \left(\Delta z_i F_{i+1} - \Delta z_{i+1} F_i \right), \tag{4}$$

where the trapezoidal rule is employed to compute the dissipated energy as the area enclosed by the hysteresis loop, with $(z_{n+1}, F_{n+1}) =$



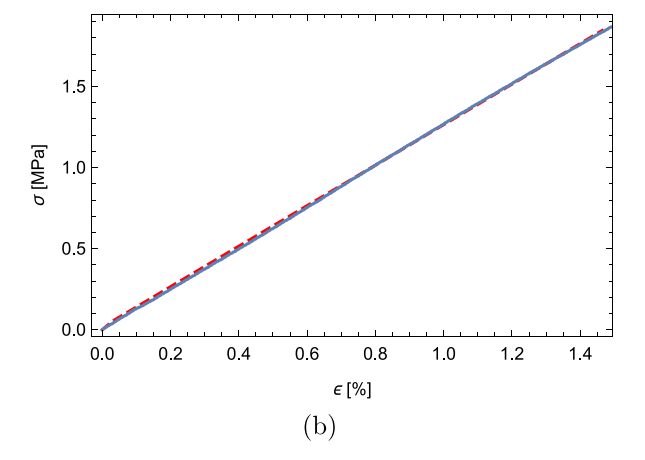


Fig. 6. (a) Membrane geometry in Yade DEM simulation (width \times height: 37×12 particles). (b) Uniaxial stretching results of the membrane: Yade DEM model (red dashed) vs. experiment (blue).

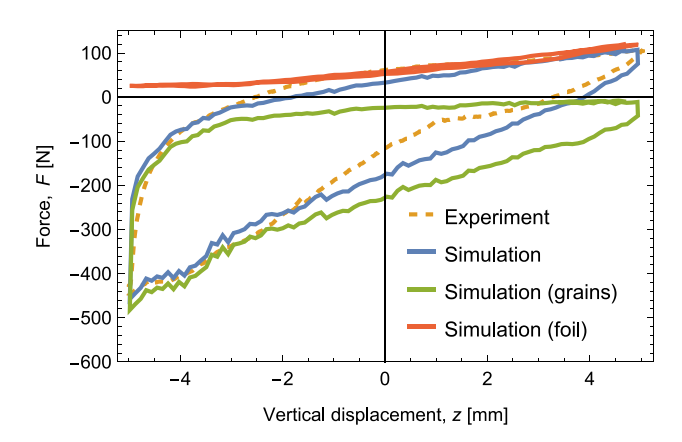


Fig. 7. Comparison of the prediction of the calibrated model and the experimental response for $\Delta p=0.06$ MPa. The simulated response force is additionally broken down into the individual contributions from foil and grains (granulate).

 (z_1, F_1) . The effective loading stiffness, k, is defined as the slope of a linear fit to the compression part of the hysteresis loop (first n/2 points):

$$(k, F_0) = \underset{(k, F_0)}{\operatorname{argmin}} \sum_{i=1}^{n/2} \left(k z_i + F_0 - F_i \right)^2, \tag{5}$$

where F_0 is the intercept, not used in our analysis. Both metrics are presented in Fig. 9 and indicate that accuracy is maintained across the vacuum pressure cases not used in the calibration, thereby further demonstrating the robustness and generalization capabilities of the calibrated DEM model.

4.3. Parametric study

The calibrated DEM model is now used to study the influence of selected material, design, and process parameters on the performance of VPP dampers. The first analyzed parameter is the friction coefficient between the granulate particles—already employed during the calibration of the DEM model; see Section 4.2. As shown in Fig. 10, modulating friction allows control over the hysteresis loop, and consequently, over the dissipative properties of VPP dampers. This effect on dissipation is strongly nonlinear: initially, even a slight increase in the friction coefficient significantly changes the hysteresis loops; however, beyond a certain point, further increases in friction have only a minor impact on dissipation (see Fig. 10(b)). For the studied case, changing the friction

coefficient from 0.6 to 1.0 results in only a few percent difference in the energy dissipation capacity of the VPP damper. Another interesting observation is the dissipative behavior at $\mu_{\bf k}=0$, which supports the hypothesis that the dynamic reorganization of the jammed particle system is responsible for dissipative effects. In summary, the friction coefficient between particles is an important factor in designing VPP dampers with desired properties.

The second studied material property of the system is the elastic modulus of particles. Fig. 11 illustrates the impact of Young's modulus on the overall dissipative characteristics of the VPP damper. Similarly to the previously described case of the friction coefficient, the influence of elastic modulus on energy dissipation capability is clearly visible. Again, a nonlinear relationship can be observed. Increasing stiffness tenfold, from 23 to 230 MPa, significantly affects the damping efficiency of the sample; however, this effect saturates beyond a certain threshold. Such behavior is, to some extent, intuitive. For conglomerates made of compliant grains, such as silicones, gels, or soft rubbers, the particles deform considerably under combined multi-axial loading. Consequently, the particle conglomerate tends to deform as a whole rather than reorganize, which effects in reducing damping effects. In contrast, the use of granulates of higher stiffness promotes the rearrangement of grains as the main mechanism of the conglomerate's deformation, resulting in an intensive dissipative response. Note that this observation partially supports the hypothesis that the dynamic rearrangement is the main dissipative mechanism in VPP systems. More direct evidence could be provided by an experimental validation for the case of softer particles. We see this as an interesting avenue for future research.

Now, we are going to study the effect of the imposed oscillation rate, which is a process parameter that describes the speed of linear displacement of the grips in the uniaxial testing machine. The sensitivity of the simulated VPP damper response to the loading velocity is illustrated in Fig. 12. According to the DEM model results, the strain rate does not significantly influence the predicted global dissipative properties of the VPP dampers. These results align with expectations since, in the DEM model, both the material properties of the foil and particles are linearly elastic, and the Coulomb friction model employed is rate-independent. Consequently, the numerical model is not expected to directly exhibit any viscous or rate-dependent effects over a wide range of loading velocities. The dominating dissipative mechanism is through the rearrangement of particles, having its roots in the damping of the kinetic energy of particles released from the jammed state. This rate-independent nature of VPP dampers is also partially confirmed by experimental study [20] for different family of VPP dampers, which additionally justifies the modeling assumptions of the present model. However, we expect that for real system, imposing

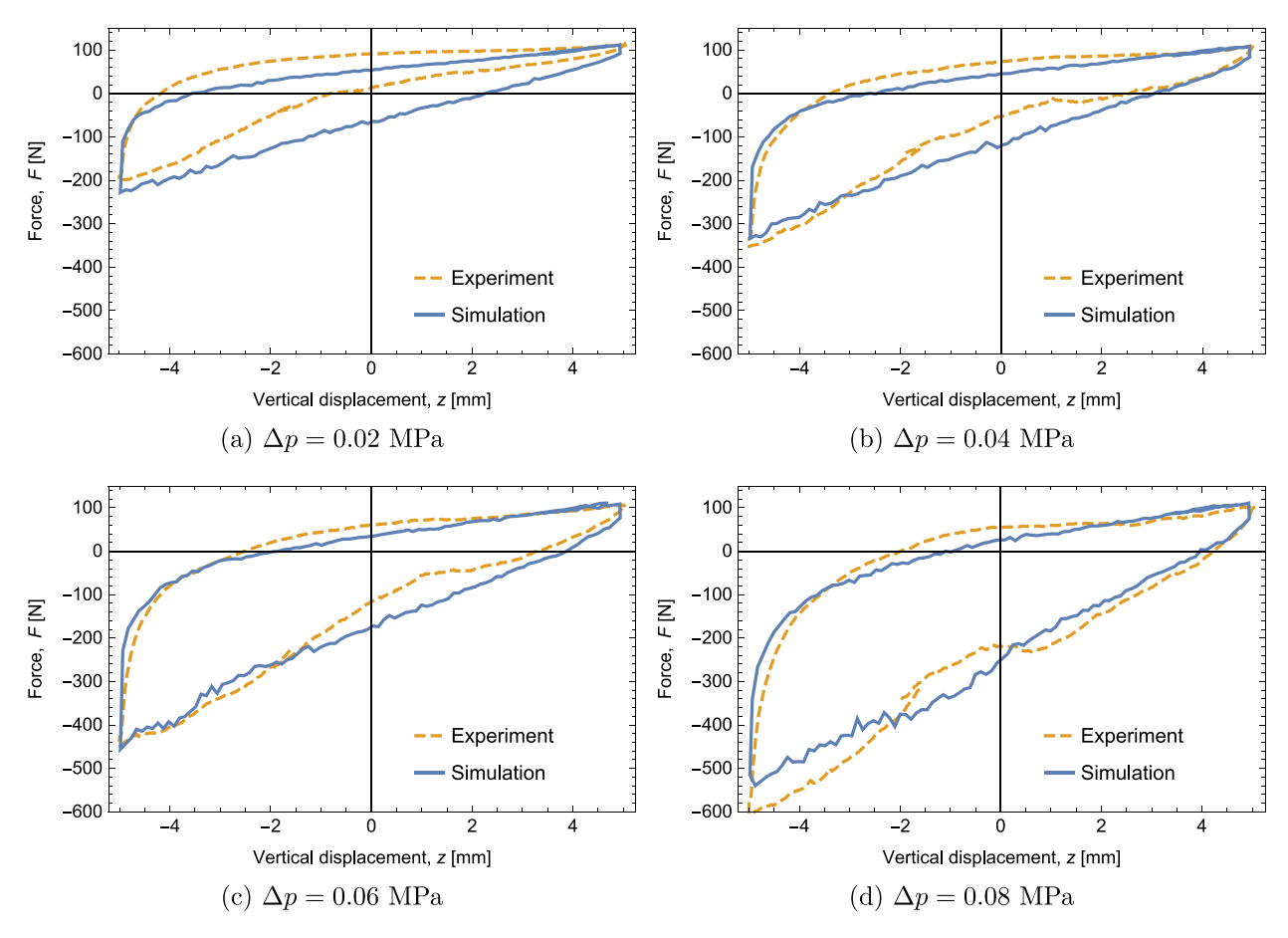


Fig. 8. Performance of the calibrated model in reproducing hysteresis loops at different vacuum pressures: (a) $\Delta p = 0.02$ MPa, (b) $\Delta p = 0.04$ MPa, (c) $\Delta p = 0.06$ MPa (the case used for calibration), (d) $\Delta p = 0.08$ MPa.

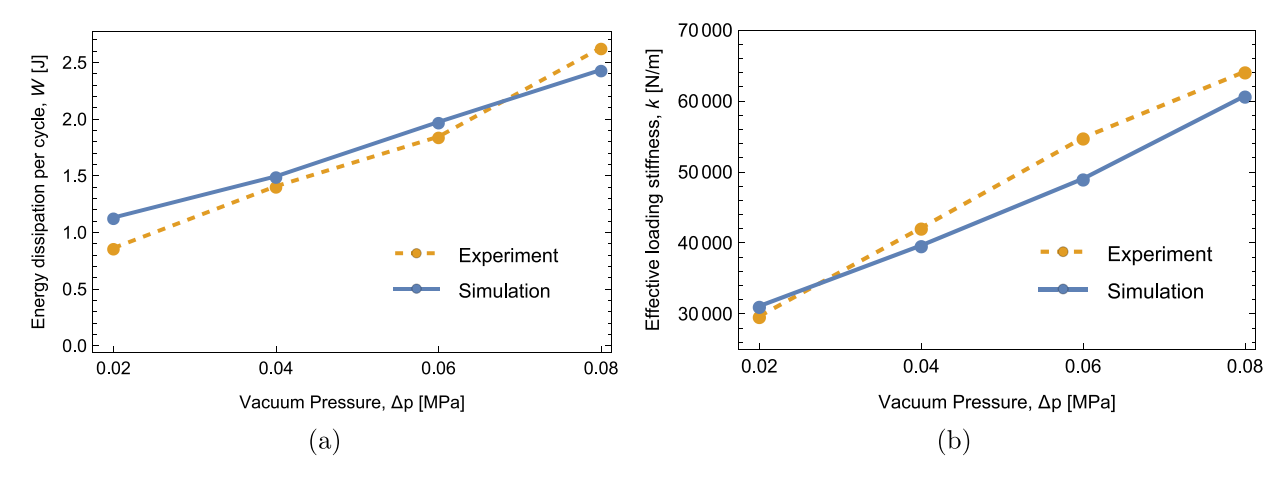


Fig. 9. Performance of the calibrated model expressed by two metrics at different vacuum pressures: (a) energy dissipation per cycle and (b) effective loading stiffness coefficient.

more pronounced oscillation rates can indeed result in differences in the shape of hysteresis loop. This effect can be caused either by the insufficient performance of the vacuum pump (already mentioned in Section 4.2) or by an increased coupling between the global response and the local dissipation of particles' kinetics. A dedicated experiment for such high-velocity deformation cases can be an interesting topic for

future study, which will provide a better evidence on applicability of VPP dampers in dynamic environments.

Finally, we demonstrate how changing the geometry of VPP dampers affects their dissipative performance. To illustrate this, we vary the damper radius, $r_{\rm p}$, and measure the total energy dissipated per cycle, expecting it to increase with radius. To quantify the *efficiency* of

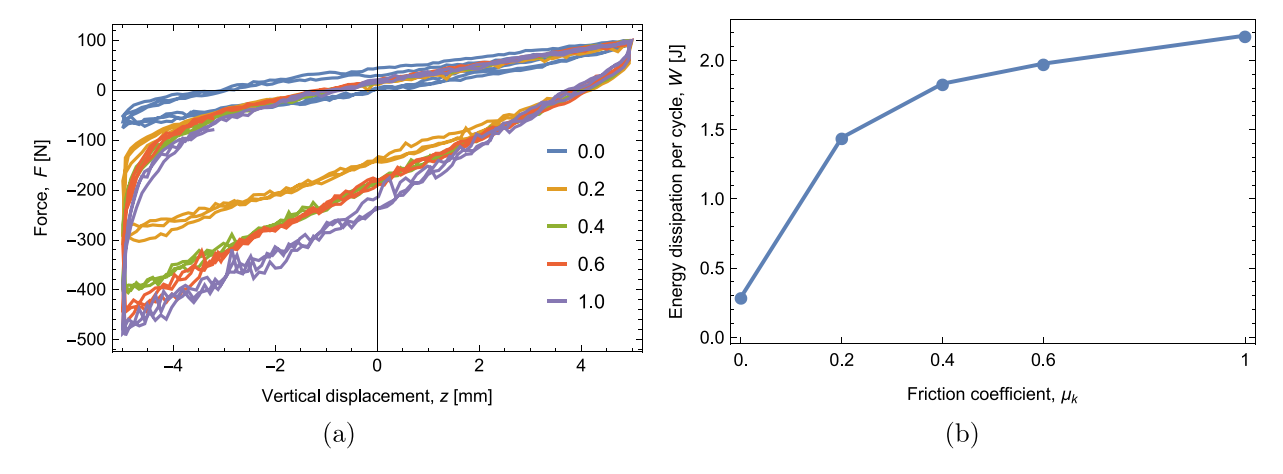


Fig. 10. Parametric study of the model response to the granulate friction coefficient μ_k . (a) Hysteresis loops, and (b) energy dissipation per cycle. Vacuum pressure $\Delta p = 0.06$ MPa.

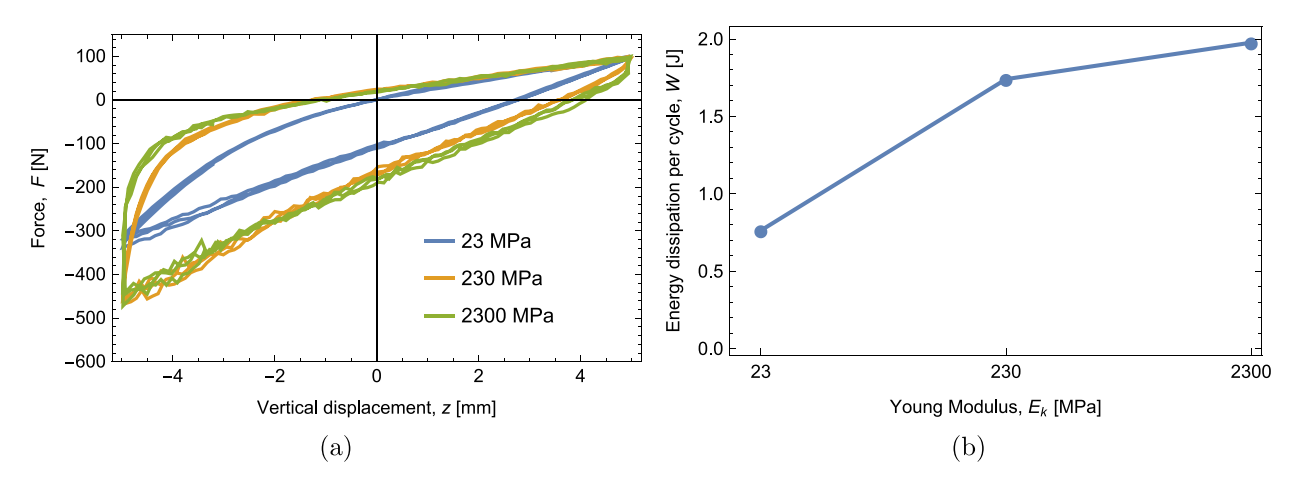


Fig. 11. Parametric study of the model response to the Young modulus of the grains inside the core. (a) Hysteresis loops, and (b) energy dissipation per cycle. Vacuum pressure $\Delta p = 0.06$ MPa.

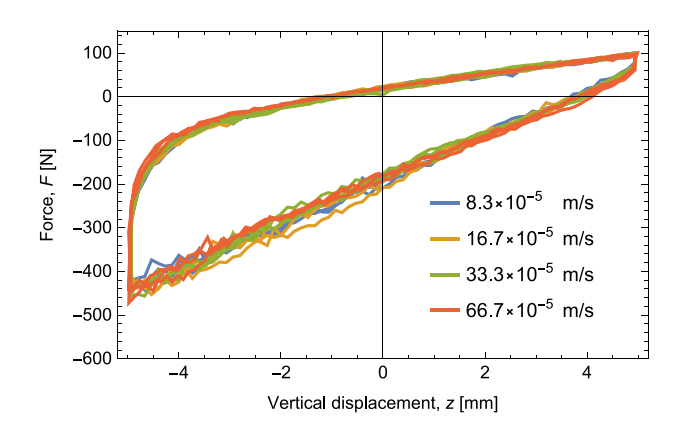


Fig. 12. Parametric study of the model response to loading velocity, $v_z.$ Vacuum pressure $\Delta p=0.06$ MPa.

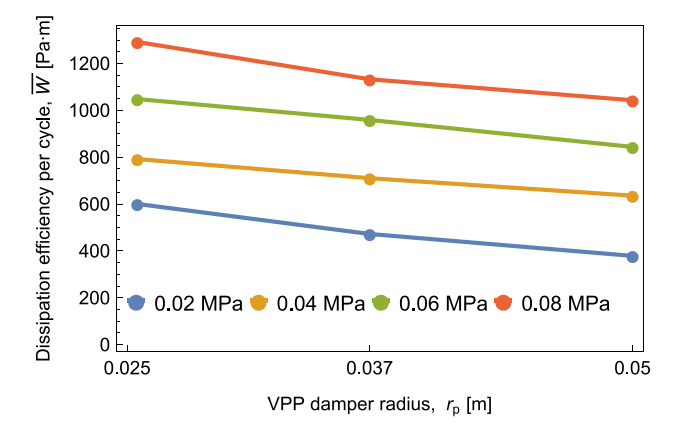


Fig. 13. Analysis of the effect of sample radius, $r_{\rm p}$, on the damping efficiency, \overline{W} , for four different levels of vacuum pressure, Δp . The base radius used in all earlier examples is $r_{\rm p}=0.0255$ m.

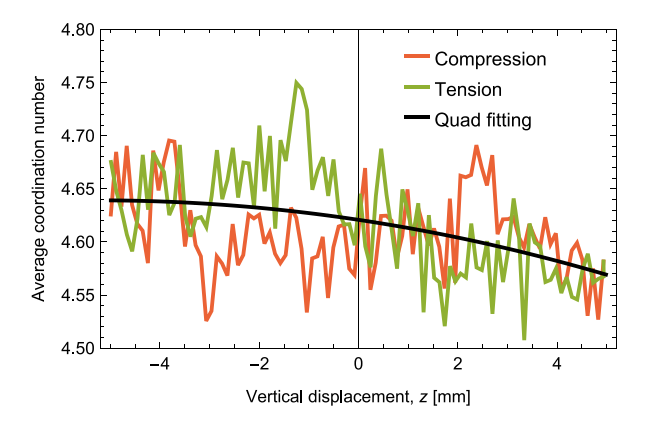


Fig. 14. Evolution of the average coordination number of granulate over a single loading cycle, for the vacuum pressure $\Delta p = 0.06$ MPa.

energy dissipation per cycle, \overline{W} , the total dissipated energy per cycle, W, given by Eq. (4), is normalized by the damper's cross-sectional area, $s_s = \pi r_p^2$:

$$\overline{W} = \frac{W}{s_s}. (6)$$

Results for three damper radii and four distinct underpressure levels are presented in Fig. 13. It is evident that increasing the damper's radius at constant height reduces the energy dissipation efficiency, a trend consistent across all analyzed underpressure levels. Consequently, to enhance dissipation performance, stacking multiple slender VPP dampers is preferable to using a single damper with a larger radius.

Although the results of this parametric study are based solely on numerical simulations, they align with certain experimental observations. For example, in our earlier work [64,65], we observed that stiffer granular materials (e.g., PMMA) enhance the energy dissipation capacity of VPP dampers. A more systematic experimental investigation is, however, still required to disentangle the various factors influencing damper performance, which remains the focus of our ongoing research.

Remark. This study focused on the macroscopic (effective) properties of VPP dampers, motivated by the (partial) availability of corresponding experimental results. Nevertheless, the calibrated DEM model is also capable of providing detailed insights into microstructural effects. For example, the displacement maps in Fig. 5(b–c) suggest the formation of shear bands, which may indicate localized zones of elevated dissipation. Likewise, the evolution of the coordination number shown in Fig. 14 indicates limited compaction during compression, which is largely reversible upon unloading. A systematic investigation of such microstructural effects lies beyond the present scope, but is planned as an important direction for future work.

5. Conclusions and future work

In this work, we proposed a novel approach to modeling Vacuum Packed Particles (VPP). In contrast to the commonly adopted phenomenological models, which treat VPP systems as continua, we employed a fully discrete framework. The Discrete Element Method (DEM) was used to model not only the granular core but also the continuous elastic membrane that separates the granulate from the external environment and transmits the pressure difference induced by the applied vacuum. The membrane was represented as a system of interconnected spherical particles, with a dedicated model developed to impose the corresponding surface forces. A dedicated VPP damper prototype was built, and a series of experiments were conducted to calibrate the model parameters and validate the simulation results. The calibrated DEM model was shown to generalize well to underpressure

levels not included in the fitting procedure. Furthermore, a parametric study was conducted to analyze the influence of material, process, and geometrical design parameters on the macroscopic response of VPP-based systems, demonstrating the capability of the proposed approach for the tuning and optimization of VPP dampers.

Several directions for future research have been identified. The most immediate continuation would involve a more extensive parametric study, encompassing both DEM simulations and corresponding experimental validation. For instance, high-frequency, step or impulse input tests could evaluate transient response of the VPP dampers, assess their applicability for dynamic environments, and reveal additional effects not captured by the present model. Another promising direction is a more detailed analysis of the microscopic mechanisms responsible for macroscopic dissipation, in particular the respective contributions of frictional sliding and dynamic particle reorganization. The developed DEM model offers a suitable framework for these studies. In addition, extending the framework to account for non-spherical particle shapes - an area in which our group has prior experimental and numerical experience - would allow more realistic modeling of angular or interlocking granulates. DEM formulations such as clumps, polyhedra, or signed distance field (SDF)-based particles [66] offer promising avenues to explore in this regard, and we see their application to VPP dampers as a highly relevant direction for future work. Finally, the development of machine learning-based surrogate models may offer significant acceleration of predictions while maintaining the required accuracy. In this context, graph neural network architectures appear particularly well-suited [67–70].

All code, together with the experimental and simulation datasets, is made available in open-access repositories [58,59]. These resources are intended to facilitate reproducibility, enable further comparative studies, and serve as a foundation for future developments in both academic and industrial contexts related to particle damping, granular materials modeling, and discrete element simulations. The present work also constitutes a part of the ongoing research efforts within our group, aimed at advancing the modeling, analysis, and optimization of granular-based damping systems. We hope that by sharing these developments, we can contribute to the broader community of researchers and practitioners working in the fields of granular systems, particle mechanics, and structural dynamics.

CRediT authorship contribution statement

Pawel Chodkiewicz: Writing – review & editing, Writing – original draft, Visualization, Validation, Software, Methodology, Investigation, Formal analysis, Data curation, Conceptualization. Robert Zalewski: Writing – review & editing, Writing – original draft, Validation, Supervision, Resources, Project administration, Methodology, Investigation, Funding acquisition, Formal analysis, Conceptualization. Jakub Lengiewicz: Writing – review & editing, Writing – original draft, Visualization, Validation, Supervision, Software, Resources, Project administration, Methodology, Investigation, Formal analysis, Conceptualization.

Declaration of competing interest

The authors declare that they have no known competing financial interests or personal relationships that could have appeared to influence the work reported in this paper.

Data availability

We have shared links to codes and data in the open-access repositories.

References

- Schwab Klaus. The fourth industrial revolution. New York, NY: Crown Publishing Group: 2017.
- [2] Elfaleh Issam, Abbassi Fethi, Habibi Mohamed, Ahmad Furqan, Guedri Mohamed, Nasri Mondher, Garnier Christian. A comprehensive review of natural fibers and their composites: An eco-friendly alternative to conventional materials. Results Eng. 2023;19:101271.
- [3] Kumar Nishant, Luding Stefan. Memory of jamming-multiscale models for soft and granular matter. Granul Matter 2016;18(3).
- [4] Behringer Robert P, Chakraborty Bulbul. The physics of jamming for granular materials: a review. Rep Progr Phys 2018;82(1):012601.
- [5] Blanc Loïc, François Bertrand, Delchambre Alain, Lambert Pierre. Characterization and modeling of granular jamming: models for mechanical design. Granul Matter 2021;23:1–13.
- [6] Brigido-González J David, Burrow Steve G, Woods Benjamin KS. Switchable stiffness morphing aerostructures based on granular jamming. J Intell Mater Syst Struct 2019;30(17):2581–94.
- [7] Li Lvzhou, Liu Zheyu, Zhou Ming, Li Xinxin, Meng Yonggang, Tian Yu. Flexible Adhesion control by modulating backing stiffness based on jamming of granular materials. Smart Mater Struct 2019;28(11):115023.
- [8] Gagnon Louis, Morandini Marco, Ghiringhelli Gian Luca. A review of particle damping modeling and testing. J Sound Vib 2019;459:114865.
- [9] Rodak Dominik, Żurawski Mateusz, Gmitrzuk Michał, Starczewski Lech. Possibilities of vacuum packed particles application in blast mitigation seats in military armored vehicles. Bull Pol Acad Sci Tech Sci 2022;70(1).
- [10] Loeve Ario, Breedveld Paul, Dankelman Jenny. Scopes too flexible... and too stiff. IEEE Pulse 2010;1(3):26-41.
- [11] Loeve Arjo J, van de Ven Oscar S, Vogel Johan G, Breedveld Paul, Dankel-man Jenny. Vacuum packed particles as flexible endoscope guides with controllable rigidity. Granul Matter 2010;12:543–54.
- [12] Pinto R, Abreu P, Carneiro J Falcão, Restivo T. Hand rehabilitation and haptic surfaces: a tentative prototype. IFAC-PapersOnLine 2019;52(27):427–33.
- [13] Zalewski Robert, Rutkowski Michał. New controllable sound absorbers made of vacuum packed particles. In: New contributions in information systems and technologies: volume 2. Springer; 2015, p. 299–309.
- [14] Bartkowski Piotr, Zalewski Robert. A concept of smart multiaxial impact damper made of vacuum packed particles. In: MATEC web of conferences. vol. 157, EDP Sciences; 2018, p. 05001.
- [15] Bartkowski Piotr. Badania empiryczne i modelowanie dyssypatorów energii wykorzystujących pakowane próżniowo granulaty [Ph.D. thesis], Warsaw Univerity of Technology; 2019.
- [16] Brown Eric, Rodenberg Nicholas, Amend John, Mozeika Annan, Steltz Erik, Zakin Mitchell R, Lipson Hod, Jaeger Heinrich M. Universal robotic gripper based on the jamming of granular material. Proc Natl Acad Sci 2010;107(44):18809–14.
- [17] Jiang Allen, Xynogalas Georgios, Dasgupta Prokar, Althoefer Kaspar, Nanayakkara Thrishantha. Design of a variable stiffness flexible manipulator with composite granular jamming and membrane coupling. In: 2012 IEEE/RSJ international conference on intelligent robots and systems. IEEE; 2012, p. 2022-7.
- [18] Kim Sangbae, Laschi Cecilia, Trimmer Barry. Soft robotics: a bioinspired evolution in robotics. Trends Biotechnol 2013;31(5):287–94.
- [19] Zalewski R, Chodkiewicz P, Shillor M. Vibrations of a mass-spring system using a granular-material damper. Appl Math Model 2016;40(17):8033–47.
- [20] Rodak Dominik, Żurawski Mateusz, Pyrz Mariusz, Zalewski Robert. Modelling and identification of hysteresis of vacuum packed particles torsional damper. J Sound Vib 2025;616:119203.
- [21] Zalewski Robert. Modelowanie i badania wpływu podciśnienia na właściwości mechaniczne specjalnych struktur granulowanych. Wydawnictwo Komunikacji i Lacznosci; 2013.
- [22] Zalewski Robert, Chodkiewicz Paweł. Gubanov model for vacuum packed particles. In: Mechatronics 2013. Springer; 2014, p. 57–63.
- [23] Zalewski Robert, Szmidt Tomasz. Application of special granular structures for semi-active damping of lateral beam vibrations. Eng Struct 2014;65:13–20.
- [24] Benson David J. The history of LS-DYNA. 2009.
- [25] Planchard David C. SOLIDWORKS 2022 tutorial. Mission, KS: SDC Publications; 2022.
- [26] Cundall PA. Formulation of a three-dimensional distinct element model—Part I. A scheme to detect and represent contacts in a system composed of many polyhedral blocks. Int J Rock Mech Min Sci Geomech Abstr 1988;25(3):107–16.
- [27] Cundall Peter A, Hart Roger D. Numerical modelling of discontinua. Eng Comput 1992;9(2):101–13.
- [28] Fern J, Rohe A, Soga K, Alonso E. The material point method for geotechnical engineering: A practical guide. CRC Press; 2019.
- [29] Cremonesi Massimiliano, Franci Alessandro, Idelsohn Sergio, Oñate Eugenio. A state of the art review of the particle finite element method (PFEM). Arch Comput Methods Eng 2020;27(5):1709–35.

- [30] Abdallah Ali, Vincens Eric, Magoariec Hélène, Picault Christophe. DEM filtration modelling for granular materials: Comparative analysis of dry and wet approaches. Int J Numer Anal Methods Geomech 2024;48(3):870–86.
- [31] Abdallah Ali. Filtration in granular materials with non-spherical particle shapes [Ph.D. thesis], Ecole Centrale de Lyon; 2023.
- [32] Abdi Rezvan, Krzaczek Marek, Tejchman J. Simulations of high-pressure fluid flow in a pre-cracked rock specimen composed of densely packed bonded spheres using a 3D CFD model and simplified 2D coupled CFD-DEM approach. Powder Technol 2023;417:118238.
- [33] Nisar F, Rojek J, Nosewicz S, Szczepański J, Kaszyca K, Chmielewski M. Discrete element model for effective electrical conductivity of spark plasma sintered porous materials. Comput Part Mech 2024;1–11.
- [34] Bajkowski Jacek Mateusz, Dyniewicz Bartłomiej, Bajer Czesław I. Damping properties of a beam with vacuum-packed granular damper. J Sound Vib 2015;341:74–85.
- [35] Holobut Pawel, Kursa Michal, Lengiewicz Jakub. A class of microstructures for scalable collective actuation of programmable matter. In: 2014 IEEE/RSJ international conference on intelligent robots and systems. IEEE; 2014, p. 3919–25.
- [36] Lengiewicz Jakub, Kursa Michał, Hołobut Paweł. Modular-robotic structures for scalable collective actuation. Robotica 2017;35:787–808.
- [37] Piranda Benoît, Chodkiewicz Paweł, Hołobut Paweł, Bordas Stéphane PA, Bourgeois Julien, Lengiewicz Jakub. Distributed prediction of unsafe reconfiguration scenarios of modular robotic programmable matter. IEEE Trans Robot 2021;37(6):2226–33.
- [38] Benniou Hicham, Accary Abdallah, Malecot Yann, Briffaut Matthieu, Daudeville Laurent. Discrete element modeling of concrete under high stress level: influence of saturation ratio. Comput Part Mech 2021;8:157–67.
- [39] Cui Xinzhuang, Li Xiangyang, Du Yefeng, Bao Zhenhao, Zhang Xiaoning, Hao Jianwen, Hu Yangyu. Macro-micro numerical analysis of granular materials considering principal stress rotation based on DEM simulation of dynamic hollow cylinder test. Constr Build Mater 2024;412:134818.
- [40] Khakpour Mehran, Mirghasemi Ali Asghar. Macro-micro mechanical study of principal stress rotation in granular materials using DEM simulations of hollow cylinder test. Powder Technol 2023;425:118580.
- [41] Song Shunxiang, Wang Pei, Yin Zhenyu, Cheng Yi Pik. Micromechanical modeling of hollow cylinder torsional shear test on sand using discrete element method. J Rock Mech Geotech Eng 2024.
- [42] Chourdakis Gerasimos, Davis Kyle, Rodenberg Benjamin, Schulte Miriam, Simonis Frédéric, Uekermann Benjamin, Abrams Georg, Bungartz Hans-Joachim, Cheung Yau Lucia, Desai Ishaan, Eder Konrad, Hertrich Richard, Lindner Florian, Rusch Alexander, Sashko Dmytro, Schneider David, Totounferoush Amin, Volland Dominik, Vollmer Peter, Koseomur Oguz Ziya. preCICE v2: A sustainable and user-friendly coupling library. Open Res Eur 2022;2:51.
- [43] Adhav Prasad, Besseron Xavier, Peters Bernhard. Development of 6-way CFD-DEM-FEM momentum coupling interface using partitioned coupling approach. Results Eng 2024;22:102214.
- [44] Adhav Prasad. An innovative and accurate technology for multi-physics digital twins in high-performance computing [Ph.D. thesis], Unilu - University of Luxembourg [Faculty of Science, Technology and Medicine], Esch-sur-Alzette, Luxembourg; 2024.
- [45] Mohamed Tarek, Duriez Jérôme, Veylon Guillaume, Peyras Laurent. Flexible membrane boundary condition DEM-FEM for drained and undrained monotonic and cyclic triaxial tests. Granul Matter 2024;26(4).
- [46] De Bono J, McDowell G, Wanatowski Dariusz. Discrete element modelling of a flexible membrane for triaxial testing of granular material at high pressures. Géotech Lett 2012;2(4):199–203.
- [47] Cil Mehmet B, Alshibli Khalid A. 3D analysis of kinematic behavior of granular materials in triaxial testing using DEM with flexible membrane boundary. Acta Geotech 2014;9(2):287–98.
- [48] Qu Tongming, Feng YT, Wang Yong, Wang Min. Discrete element modelling of flexible membrane boundaries for triaxial tests. Comput Geotech 2019;115:103154.
- [49] Qin Yan, Liu Chun, Zhang Xiaoyu, Wang Xingang, Shi Bin, Wang Yue, Deng Shang. A three-dimensional discrete element model of triaxial tests based on a new flexible membrane boundary. Sci Rep 2021;11(1):4753.
- [50] Huang Shihao, Qian Yu, Shan Yao. Effect of flexible membrane in large-scale triaxial test DEM simulations. Constr Build Mater 2023;370:130608.
- [51] Asadi Reza, Disfani Mahdi M, Ghahreman-Nejad Behrooz, Ciantia Matteo O. Effect of flexible membrane in triaxial test on the mechanical behaviour of rockfill material using discrete element method. Granul Matter 2024;26(3):70.
- [52] Chodkiewicz Paweł, Lengiewicz Jakub, Zalewski Robert. Discrete element method approach to modelling VPP dampers. In: MATEC web of conferences. vol. 157, 2018
- [53] Kozicki J, Donzé FV. A new open-source software developed for numerical simulations using discrete modeling methods. Comput Methods Appl Mech Engrg 2008;197(49):4429-43.

- [54] Smilauer Vaclav, Angelidakis Vasileios, Catalano Emanuele, Caulk Robert, Chareyre Bruno, Chèvremont William, Dorofeenko Sergei, Duriez Jerome, Dyck Nolan, Elias Jan, Er Burak, Eulitz Alexander, Gladky Anton, Guo Ning, Jakob Christian, Kneib Francois, Kozicki Janek, Marzougui Donia, Maurin Raphael, Modenese Chiara, Pekmezi Gerald, Scholtès Luc, Sibille Luc, Stransky Jan, Sweijen Thomas, Thoeni Klaus, Yuan Chao. Yade documentation.
- [55] Mackojc Anna, Chilinski Bogumil, Zalewski Robert. Preliminary research of a symmetrical controllable granular damper prototype. Bull Pol Acad Sci Tech Sci 2022:e141002.
- [56] Bartkowski Piotr, Suwała Grzegorz, Zalewski Robert. Temperature and strain rate effects of jammed granular systems: experiments and modelling. Granul Matter 2021;23(4):79.
- [57] Šmilauer V, Catalano E, Chareyre B, et al. Yade documentation 2nd ed (the Yade project, 2015). 2015.
- [58] Chodkiewicz Paweł, Zalewski Robert, Lengiewicz Jakub. Discrete element method model of vacuum packed particle dampers. 2025, GitHub source repository: https://github.com/chpawel/VPP.
- [59] Chodkiewicz Paweł, Zalewski Robert, Lengiewicz Jakub. Discrete element method model of vacuum packed particle dampers. 2025, Zenodo dataset: https://doi. org/10.5281/zenodo.14917354.
- [60] Cundall Peter A, Strack Otto DL. A discrete numerical model for granular assemblies. Geotechnique 1979;29(1):47–65.
- [61] Williams R. Circle packings, plane tessellations, and networks. Geom Found Nat Struct: A Source Book of Des 1979;34–47.

- [62] Blokhuis A. Sphere packings, lattices and groups (grundlehren der mathematischen wissenschaften 290). Bull Lond Math Soc 1989;21(5):496–7.
- [63] Steinhaus Hugo. Mathematical Snapshots. Courier Corporation; 1999.
- [64] Zalewski Robert. Constitutive model for special granular structures. Int J Non-Linear Mech 2010;45(3):279–85.
- [65] Zalewski Robert, Pyrz Mariusz. Modeling and parameter identification of granular plastomer conglomerate submitted to internal underpressure. Eng Struct 2010;32(8):2424–31.
- [66] Lai Zhengshou, Feng YT, Zhao Jidong, Huang Linchong. Unifying the contact in signed distance field-based and conventional discrete element methods. Comput Geotech 2024;176:106764.
- [67] Sanchez-Gonzalez Alvaro, Godwin Jonathan, Pfaff Tobias, Ying Rex, Leskovec Jure, Battaglia Peter. Learning to simulate complex physics with graph networks. In: Daumé Hal, Singh Aarti, editors. Proceedings of the 37th international conference on machine learning. Proceedings of machine learning research, vol. 119, PMLR; 2020, p. 8459–68.
- [68] Choi Yongjin, Kumar Krishna. Graph neural network-based surrogate model for granular flows. Comput Geotech 2024;166:106015.
- [69] Li Shuo, Sakai Mikio. Advanced graph neural network-based surrogate model for granular flows in arbitrarily shaped domains. Chem Eng J 2024;500:157349.
- [70] Deshpande Saurabh, Bordas Stéphane PA, Lengiewicz Jakub. MAgNET: A graph U-Net architecture for mesh-based simulations. Eng Appl Artif Intell 2024;133:108055.